



ELSEVIER

Contents lists available at ScienceDirect

Nuclear Medicine and Biology

journal homepage: www.elsevier.com/locate/nucmedbioPreclinical evaluation of [^{18}F]D3FSP, deuterated AV-45, for imaging of β -amyloid in the brainZhihao Zha^{a,b}, Karl Ploessl^a, Seok Rye Choi^a, David Alexoff^a, Hank F. Kung^{a,b,*}^a Five Eleven Pharma Inc., Philadelphia, PA 19104, USA^b Department of Radiology, University of Pennsylvania, Philadelphia, PA 19104, USA

ARTICLE INFO

Article history:

Received 25 February 2020

Received in revised form 13 March 2020

Accepted 18 March 2020

Available online xxxxx

Keywords:

Alzheimer's disease

Amyvid

Deuterium

In vivo metabolism β -Amyloid

ABSTRACT

Introduction: Since the approval of three ^{18}F labeled β -amyloid-targeting PET imaging agents, Amyvid (florbetapir f18, AV-45), Neuraceq (florbetaben f18, AV-1) and Vizamyil (flutemetamol f18, F-PIB), they have increasingly been employed to assist differential diagnosis of Alzheimer's disease in patients with dementia. Also, they are frequently used in selecting patients participating drug trials aiming to reduce β -amyloid ($\text{A}\beta$) plaques in the brain. The first approved tracer in this class was [^{18}F]AV-45, which is metabolized rapidly in blood and some of its *N*-demethylated metabolites cross the blood brain barrier and resulted in lowering the image contrast. To improve metabolic stability of [^{18}F]AV-45, we hypothesized that substituting *N*- CH_3 with *N*- CD_3 at the metabolically labile position, creating [^{18}F]D3FSP, may reduce *in vivo* *N*-demethylation. We report the preclinical evaluation of [^{18}F]D3FSP as an $\text{A}\beta$ imaging agent.

Methods: Preclinical pharmacology of [^{18}F]D3FSP was evaluated using *in vitro* autoradiography and competitive binding assay. Biodistribution of [^{18}F]D3FSP was evaluated in wild-type CD-1 mice. *In vivo* metabolism in mice and *in vitro* microsomal metabolism were analyzed by HPLC. Single dose acute toxicity of D3FSP was also performed in rats.

Results: [^{18}F]D3FSP showed high binding affinity to β -amyloid plaques ($K_i = 3.44 \pm 1.22$ nM, a value similar as AV-45 ($K_i = 4.02 \pm 0.22$ nM)), and displayed excellent β -amyloid binding in AD brain sections consistent with known $\text{A}\beta$ regional distribution. After an *iv* injection it exhibited good initial brain uptake and fast washout in wild-type CD-1 mice. *In vitro* microsomal metabolism and *in vivo* metabolism in mice did not result in any significant differences between [^{18}F]D3FSP and [^{18}F]AV-45. No treatment-related mortality or any adverse effects were observed in single dose acute toxicity studies administered at hundred-folds of maximum human dose.

Conclusion: A new small molecule, [^{18}F]D3FSP, was prepared and tested as an alternative to [^{18}F]AV-45 to reduce *N*-demethylation *in vivo*. This strategy did not lead to better *in vivo* stability. However, [^{18}F]D3FSP displayed very similar $\text{A}\beta$ targeting property comparable to [^{18}F]AV-45. Preclinical studies suggest that [^{18}F]D3FSP is useful as a β -amyloid-targeting PET imaging agent.

© 2020 Published by Elsevier Inc.

1. Introduction

Alzheimer's disease (AD) is the most common type of dementia. It is projected that 14 million people will live with AD in the USA by 2060 [1]. AD is a progressive and fatal neurodegenerative disorder. Accumulation of β -amyloid plaques ($\text{A}\beta$) and intracellular neurofibrillary tangles (Tau) in the brain are two neuropathologic hallmarks of AD. The detection of these hallmarks has shown diagnostic and prognostic value in the management of Alzheimer's disease [2–5].

In 2012, the Food and Drug Administration (FDA) has approved a new radiopharmaceutical agent, Florbetapir F18 (Amyvid, AV-45), to assist clinicians in detecting causes of cognitive impairment other than Alzheimer's disease. Florbetapir F18 injection (AmyvidTM, Eli Lilly) is

indicated for positron emission tomographic (PET) imaging of the brain in cognitively impaired adults undergoing evaluation for Alzheimer's disease and other causes of cognitive decline [6]. The development of β -amyloid plaque-targeting radiotracers has enabled non-invasive PET imaging to quantitate β -amyloid deposition in a living human brain [7–12]. As shown in Fig. 1, three PET tracers for *in vivo* visualization of brain β -amyloid plaques have been approved for clinical use by the US Food and Drug Administration (FDA) and European Medicines Agency (EMA): [^{18}F]AV-45 ([^{18}F]florbetapir; AmyvidTM) [13], [^{18}F]AV-1 ([^{18}F]florbetaben; NeuraceqTM) and [^{18}F]3'-F-PIB ([^{18}F]flutemetamol; VizamyilTM).

Recently, β -amyloid PET imaging has become an important tool in the transformation of AD research, which could potentially accelerate therapeutic drug development [14]. β -Amyloid PET is likely to contribute to better patient care as well [15]. Recent changes in using biomarkers ($\text{A}\beta$ deposition in the brain or $\text{A}\beta$ in CSF) as a biological

* Corresponding author at: Five Eleven Pharma Inc., Philadelphia, PA 19104, USA.

E-mail address: kunghf@sunmac.spect.upenn.edu (H.F. Kung).

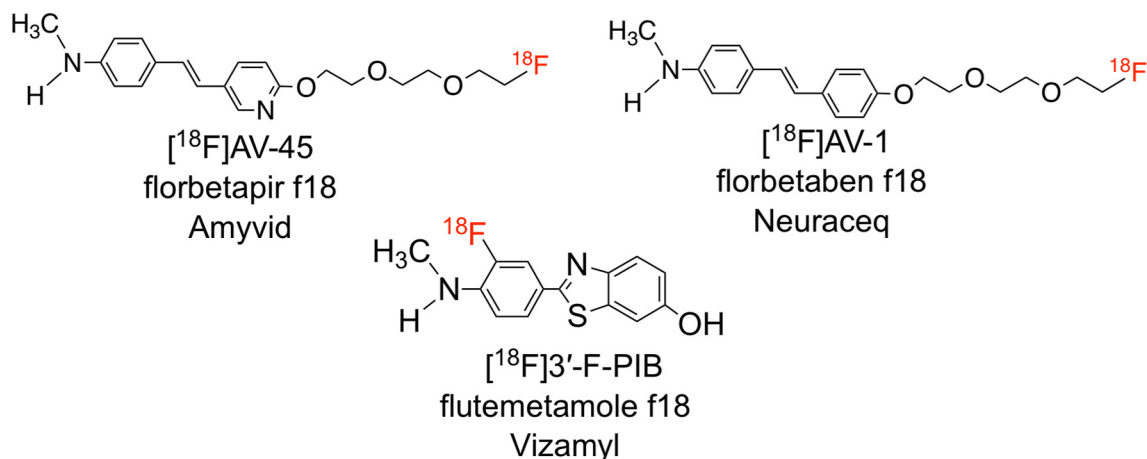


Fig. 1. Three FDA approved PET tracers, Amyvid, Neuraceq and Vizamyl, for imaging β -amyloid plaques in assisting diagnosis of Alzheimer's disease (AD).

definition of AD was announced by the National Institute on Aging and Alzheimer's Association [2,16]. New diagnostic recommendations for the preclinical, mild cognitive impairment, and dementia stages of Alzheimer's disease defined by its underlying pathologic processes can be documented by *in vivo* biomarkers, *i.e.* using β -amyloid PET imaging to measure A β load in patients [16]. Accessing the status of β -amyloid plaque accumulation in the brain by non-invasive PET imaging is critical for accurate diagnosis of AD, and also beneficial to selecting patients for developing therapy for AD. Since the first approval of $[^{18}\text{F}]\text{AV-45}$ (florbetapir f18, Amyvid) in 2012 [13], β -amyloid PET imaging agents are being utilized in a clinical setting [17,18]. They improve subject selection and treatment response monitoring for anti-amyloid therapies during early phases of the disease [19,20].

As shown in Fig. 1, all three tracers contain an *N*-methyl group which is crucial for high binding affinity to β -amyloid plaques. It was also confirmed that *N*-demethylation is one of the major pathway of metabolism in $[^{18}\text{F}]\text{AV-45}$ [12,21,22] and $[^{18}\text{F}]\text{AV-1}$ [23]. Besides *N*-demethylated derivatives, the other major radioactive metabolites were identified as the *N*-acetylated derivative $[^{18}\text{F}]\text{AV-267}$ (Fig. 2) [22]. The same metabolites were identified in human plasma [21]. Both metabolites - derived from *N*-demethylation - exhibited lower binding affinity to β -amyloid plaques, but they are capable of penetrating blood brain barrier (BBB). Therefore, the ^{18}F -metabolites in the brain could contribute to an increased nonspecific binding and lowering the specificity for detecting β -amyloid plaques in the brain. It was hypothesized that slowing down the *N*-demethylation by deuterium substitution of hydrogen might increase the brain uptake of the parent radiotracer and reduce non-specific binding by the metabolites.

Because $[^{18}\text{F}]\text{AV-45}$ and $[^{18}\text{F}]\text{AV-1}$ share close similarity in their chemical structures, they showed as expected similar pharmacokinetic and metabolic fates [23]. The preclinical and clinical PK data of both tracers showed that the radiolabeled metabolites, *N*-demethylated metabolites, may contribute significantly to the total radioactivity, and the *N*-demethylated metabolites displayed a 20 to 30-fold lower binding affinity [12,21,24] to the β -amyloid (A β) plaques in the brain (Fig. 2). Preclinical experiments suggest that these metabolites penetrate intact BBB and distribute into the brain. Slowing down *N*-demethylation could lower the metabolites entering the brain, which could contribute to an increase of specific signal measured by PET imaging.

Deuterated medications are an active area in drug development [25–27]. Various strategies to enhance metabolic stability might be used and the deuterated drug approach is one of them [28]. Deuterium (D) is a naturally-occurring, nonradioactive isotope of hydrogen (H). D has a 2-fold higher mass than H, leading to a reduced vibrational stretching frequency of the C–D bond. Also, C–D bonds are shorter than C–H bonds by 0.005 Å [27]. Therefore, the activation energy required for reaching the transition state for bond cleavage is greater for C–D than C–H, and it is harder to break C–D bonds than C–H bonds. The difference in the stability of isotopically substituted molecules is referred to as the primary kinetic isotopic effect (KIE) [29]. To observe high KIE by deuterium substitution, it is necessary that the C–H cleavage step is at least partially rate-limiting among the multistep enzyme-catalyzed metabolism. The efforts to exploit isotope effects in the design of radiotracers resulted in a mixed outcome [30–33]. Deuterium substitution in small molecules often does not result in a change of the shape,

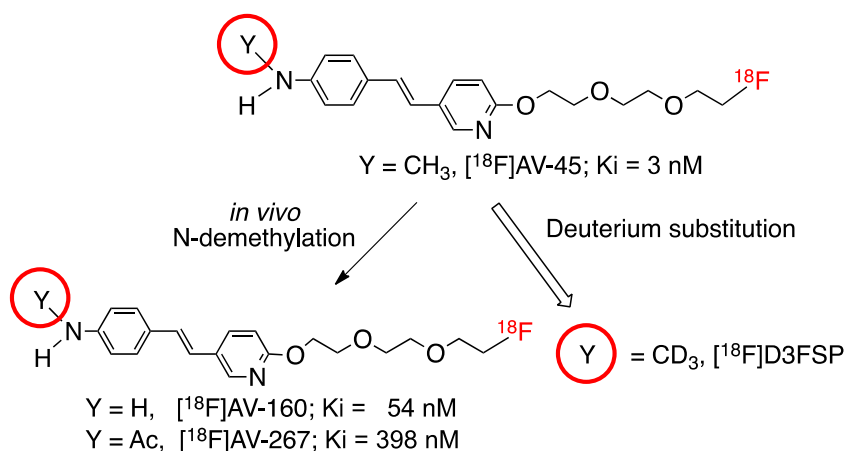


Fig. 2. Chemical structures of $[^{18}\text{F}]\text{AV-45}$, its known radioactive metabolites and $[^{18}\text{F}]\text{D3FSP}$.

size, charge or target pharmacology. However, because a carbon-deuterium chemical bond is stronger than a carbon-hydrogen bond, deuterium substitution may slow down drug metabolism. This attenuation of metabolism can lower the injection dose, lower radiation exposure and sometimes improve image contrast [27]. In 2017, FDA approved deuterotetrabenazine for the treatment of choreas associated with Huntington's disease [34], the same indications of the parent drug, tetrabenazine. This announcement provided a stamp of approval and gave an endorsement for the pharmaceutical industry to develop additional deuterated derivatives of existing drugs as new chemical entities [35].

Among many metabolic reactions catalyzed by cytochrome P450 (CYP450), amine N-dealkylation can be slowed down by deuterium substitution when N-dealkylation is the rate-limiting step in drug metabolism [36]. Mechanistic studies of model P450 enzyme catalyzed N-demethylation reactions have shown that the first step proceeds via a hydrogen atom extraction (and thus susceptible to effects of deuterium substitution), followed by oxidation reactions leading to the removal of the N-methyl group [37]. Deuterium substitution would in theory show a slower kinetics in breaking of C-D bond. It was reported that [¹⁸F]AV-1 was metabolized by several CYP enzymes. Enzyme CYP4F2 predominantly mediates N-demethylation, whereas CYP2J2 and CYP3A4 contribute predominantly to the formation of polar metabolites. Among those, CYP2J2 and CYP4F2 were identified as the main enzymes involved in the metabolism of [¹⁸F]AV-1 [38]. From the results of [¹⁸F]AV-1, it is reasonable to infer that the same CYP enzymes might also be involved in the metabolism of [¹⁸F]AV-45.

Hydrogen-deuterium substitutions have been adopted in direct proximity to [¹⁸F]fluoride to avoid ¹⁸F-defluorination [39]. A successful example of the stabilization by means of deuteration consists of the preparation of [¹⁸F]FE-(+)-DTBZ-D4 [40]. *In vivo* studies with [¹⁸F]FE-(+)-DTBZ showed high accumulation of radioactivity in joints and bones. To improve the metabolic stability, [¹⁸F]FE-(+)-DTBZ-D4 was developed and showed a six fold increase in half-life stability. The main improvement was the considerably reduced bone uptake when comparing with the non-deuterated tracer. Because [¹⁸F]AV-45 did not show significant defluorination, we have selected not to substitute fluoroalkyl chains with deuterium. The hydrogens in the N-methyl group, which are known to metabolic degradation, were chosen to substitute hydrogen on the N-methyl group with deuterium.

To address the metabolic instability of [¹⁸F]AV-45, we have synthesized a deuterated derivative of [¹⁸F]AV-45, [¹⁸F]D3FSP, in which N-methyl group that plays a key role in its *in vivo* metabolism was replaced with a N-trideuteromethyl group (-NCD₃) (Fig. 2). Replacement of hydrogen with deuterium could improve the *in vivo* stability, which could lead to better *in vivo* signal to noise ratios in the brain. Therefore, [¹⁸F]D3FSP and the 'cold' D3FSP were prepared and characterized with respect to their *in vitro* binding to Aβ plaques in postmortem AD brain tissue homogenates, *in vivo* biodistribution, *in vitro* microsomal and *in vivo* metabolism in mice, and acute toxicity in rats. We compared data of [¹⁸F]D3FSP with those of [¹⁸F]AV-45 which is an FDA approved drug with proven safety and effectiveness.

2. Results

Synthesis of D3FSP, D3AV-1 and related precursors and standards are included in the supplemental information. Results of preparation and quality controls of [¹⁸F]D3FSP and [¹⁸F]AV-45 following established procedures are also included in the supplemental information.

Radiolabeling procedures (Fig. 3) were similar to published methods for [¹⁸F]AV-45 [22]. Precursor (4) was radiolabeled with activated [¹⁸F]fluoride with K₂₂₂/K₂CO₃ in DMSO for 15 min at 110 °C. The solution was allowed to cool and the protection group was cleaved with 10% HCl solution at 100 °C for 10 min. The product, [¹⁸F]D3FSP, was then purified by semi-preparative HPLC. Activities used ranged from 442 MBq to 4.1 GBq (*n* = 8), with radiochemical purities of 98.5 ± 1.3%. Radiochemical yields (decay corrected) were 55 ± 11% with molar activities (A_m) of 22.8 ± 12.4 GBq/μmol. Similarly, [¹⁸F]AV-45 was prepared and tested for comparison with [¹⁸F]D3FSP as described in this paper.

2.1. *In vitro* competitive binding assay

In vitro binding studies, using either [¹⁸F]D3FSP or [¹⁸F]AV-45 as the "hot ligand", showed that hydrogen to deuterium substituted analog ("cold" AV-45 vs D3FSP) exhibited the same excellent binding affinity to β-amyloid plaques from AD human brain (K_i = 3 to 4 nM). No effect was observed for deuterium substitution on binding affinity; all deuterated agents, D3FSP and D3AV-1 displayed the same binding affinity as their hydrogen analogs (Table 1).

2.2. *In vitro* autoradiography of AD brain sections with [¹⁸F]D3FSP

Various postmortem AD brain sections were incubated *in vitro* with [¹⁸F]AV-45 or [¹⁸F]D3FSP to directly compare the tracer binding to β-amyloid plaques. The images of autoradiography (Fig. 4) showed a broad spectrum of varying signal intensities obtained over the tissue samples from different AD patients reflecting different levels of β-amyloid plaques. The darkly speckled band around the edge of the positive tissue sections reflects [¹⁸F]D3FSP or [¹⁸F]AV-45 labeling of β-amyloid plaques present in the gray matter, while the light central area of the tissue reflects white matter that is not specifically labeled by [¹⁸F]D3FSP or [¹⁸F]AV-45 (Fig. 4).

Blocking of [¹⁸F]D3FSP or [¹⁸F]AV-45 binding to β-amyloid plaques in these brain sections by several known β-amyloid binding ligands or self-blocking resulted in complete blocking of β-amyloid binding of both tracers (Fig. 5). Blocking studies demonstrate that [¹⁸F]D3FSP and [¹⁸F]AV-45 bind to the same sites, and the "cold" ligands - AV-45, AV-1, PIB and IMPY compete with [¹⁸F]D3FSP and [¹⁸F]AV-45 for the same binding sites.

2.3. *In vitro* liver microsomal metabolism

In vitro microsomal metabolism were conducted by incubation of [¹⁸F]D3FSP or [¹⁸F]AV-45 using the same batch of mouse and human liver microsomes. The metabolites of [¹⁸F]D3FSP or [¹⁸F]AV-45 were

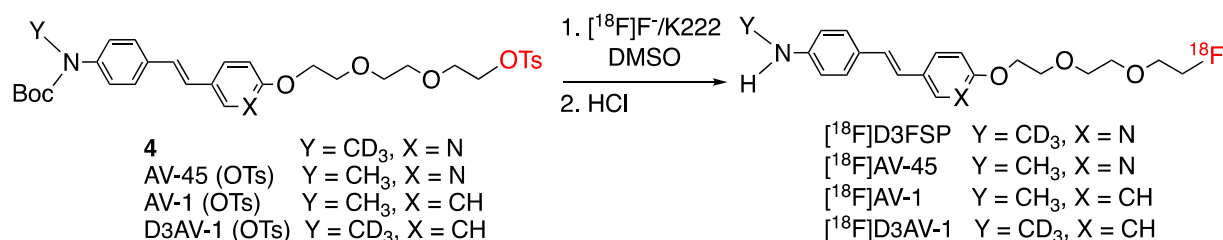
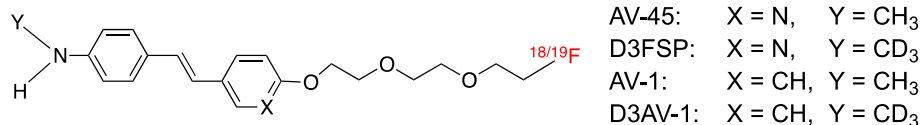


Fig. 3. Preparation of [¹⁸F]D3FSP, [¹⁸F]AV-45, [¹⁸F]AV-1 and [¹⁸F]D3AV-1.

Table 1
In vitro binding affinity to β -amyloid plaques of human AD brain homogenates (K_i , nM, Avg \pm SD, $n = 3$).



Hot ligand	K _i of cold competing drug (nM, Avg \pm SD, $n=3$)		
	D3FSP	AV-45	D3AV-1
[¹⁸ F]D3FSP	3.25 \pm 0.82	3.24 \pm 0.76	4.15 \pm 0.75
[¹⁸ F]AV-45	3.44 \pm 1.22	4.02 \pm 0.22	3.35 \pm 0.88

measured using human and mouse liver microsomes in the presence of an NADPH-generating system at 37 °C for 1, 5, 15, 30, 60 and 120 min. The radioactive incubation mixtures were extracted and assayed using HPLC, and the profiles of parent compounds and metabolites were determined by reverse-phase HPLC. Incubation with mouse liver microsomes of [¹⁸F]D3FSP and [¹⁸F]AV-45 led to four metabolites, and five metabolites were found after incubation with human liver microsomes. The rate of formation of various metabolites for [¹⁸F]D3FSP and [¹⁸F]AV-45 was analyzed by plotting the amount of the parent and each of the metabolites against incubation time (Fig. 6).

The study shows that both [¹⁸F]AV-45 and [¹⁸F]D3FSP were rapidly metabolized by human and mouse liver microsomes (Fig. 6A and B). After 30 min incubation with the mouse microsomes, only 1.5 to 3% of the parent ligands remained and the dominant metabolite was the *N*-demethylated product (M1) accounting for about 50% of the original activity. The biological half-life of [¹⁸F]AV-45 and [¹⁸F]D3FSP was estimated to be <5 min in this study. The metabolites detected after incubation of [¹⁸F]AV-45 and [¹⁸F]D3FSP in liver microsomes from mouse and human were the *N*-demethylated products, lipophilic metabolites and hydrophilic metabolites. However, the results suggest that there are no differences between [¹⁸F]D3FSP and [¹⁸F]AV-45. Both agents showed very similar pattern of metabolites qualitatively and quantitatively (Fig. 6C and D).

2.4. Biodistribution

Following an *iv* injection into the tail vein of normal mice, [¹⁸F]D3FSP distributed primarily to the liver and kidneys. Within 2 min post-injection, there was 6.3% injected dose per gram (% dose/g) in the brain. However, the activity cleared rapidly from the brain dropping to 1.7% dose/g in 30 min as shown in Table 2. Biodistribution studies of [¹⁸F]D3FSP in normal mice have shown that, as expected, it is rapidly distributed to the brain but not retained in the absence of β -amyloid deposits. Distribution and elimination from other tissues were also rapid. Excretion was mainly *via* the gastrointestinal route. The biodistribution of [¹⁸F]D3FSP (Table 2) and [¹⁸F]AV-45 (Table 3) in wild type CD-1 mice showed very similar results. Both the [¹⁸F]D3FSP and [¹⁸F]AV-45 showed comparable brain penetration at 2 min and similar brain retention at later time points (60 and 120 min). The rapid clearance from the brain without β -amyloid plaques would likely reduce non-specific binding to the brain tissue leading to less non-specific binding in imaging. Ratios of brain and blood uptake and clearance in mice of [¹⁸F]D3FSP showed an excellent initial uptake in the brain and was followed by a rapid clearance from the brain (Table 4).

2.5. *In vivo* metabolism in normal mouse

The parent activity of [¹⁸F]D3FSP and [¹⁸F]AV-45, and their radioactive metabolites from plasma and brain after *iv* injection in normal mice were analyzed using HPLC. Both [¹⁸F]D3FSP and [¹⁸F]AV-45 were rapidly metabolized into various radioactive metabolites, and the

metabolized fractions in plasma increased over time (Fig. 7. And Fig. 8). Within 30 min after injection, only 21% of the parent [¹⁸F]D3FSP was present in plasma. The profiling and identification of the metabolites was performed by HPLC with radioactive detection and comparison with the data of [¹⁸F]AV-45. [¹⁸F]-*N*-demethylated product ([¹⁸F]AV-160) and [¹⁸F]AV-267 were identified with cold standard compounds previously [22], but other hydrophilic metabolites were not characterized. Results suggested that both [¹⁸F]D3FSP and [¹⁸F]AV-45 displayed very similar *in vivo* metabolism profiles in the brain of mice. The deuterium substitution apparently did not lead to any significant changes in the metabolism in the brain of mice.

Analysis of plasma and brain extracts following *iv* administration of [¹⁸F]D3FSP or [¹⁸F]AV-45 in normal mice were performed. Radio-HPLC profiles of extracts from the brain showed three radioactive metabolite peaks along with [¹⁸F]D3FSP with retention times at 2, 9.7, 10.9, and 13.4 min, respectively (HPLC profiles see SI Fig. S4a). The pattern was again very similar to that of [¹⁸F]AV-45 (Fig. 7a and b).

On the other hand, plasma showed two more radioactive metabolite peaks with retention times at 4.3 and 16.6 min (HPLC profiles see SI Fig. S4b). The main radioactive metabolite peak eluted at 2 min was highly polar and remained to be identified. These findings are in accordance with the *in vitro* metabolites observed after incubation with mouse and human microsomes. The percentage of parent [¹⁸F]D3FSP exponentially decreased as a function of time representing 74.2 \pm 7.8% at 2 min and 20.8 \pm 2.3% at 30 min post-injection, respectively. During the same time, the percentage of the main polar ¹⁸F-metabolite increased and reached 20.9 \pm 2.3% of plasma radioactivity. Again a very similar pattern of metabolites were observed for [¹⁸F]AV-45 (Fig. 8a and b). These radioactivity peaks associated with metabolites may be due to the presence of [¹⁸F]fluoroacetate (or [¹⁸F]fluoroacetic acid) generated by *O*-dealkylation of the tracer. The major radioactive metabolite, *N*-demethylated product in plasma reached 50.8 \pm 4.0% at 60 min post-injection. Since there is no target binding site in the brain of normal mouse, the percentage of [¹⁸F]D3FSP in the brain was very low. *In vitro* microsomal metabolism and *in vivo* metabolism in mice were not significantly different between the two radiotracers, [¹⁸F]AV-45 and [¹⁸F]D3FSP; the deuterium substitution apparently did not show modification of *in vivo* metabolism.

It was stated in the package insert of Amyvid that the maximum chemical dose per injection would be 50 μ g [13]. Acute pharmacological toxicity test was performed in rats using one hundred times of estimated maximum human dose. Rats received either vehicle or 0.52 mg/kg D3FSP once on Day 1 *via iv* injection at a dose volume of 4 mL/kg. On Day 2 and Day 15 after drug administration, clinical observations, body weight measurements, blood samples for the evaluation of hematology, clinical chemistry, and coagulation endpoints and histological examinations of organs were performed. No drug related pathological findings by macroscopic or microscopic examinations in any of the animals at either sacrifice intervals were observed.

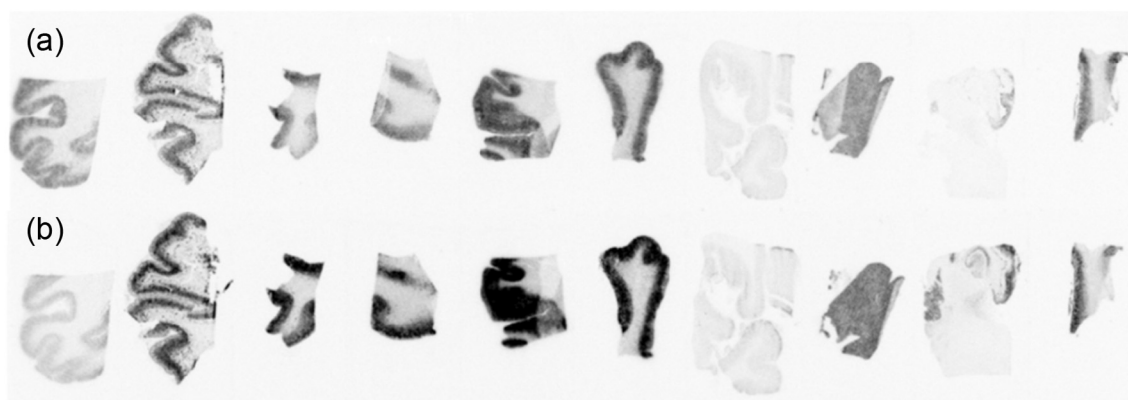


Fig. 4. Comparison of β -amyloid plaques binding between (a) [^{18}F]AV-45 and (b) [^{18}F]D3FSP and *in vitro* autoradiograms of frozen brain tissue sections from postmortem AD patients. Both tracers showed consistent and comparable β -amyloid plaque binding.

3. Discussion

Significant amount of information on *in vivo* metabolism of [^{18}F]AV-45 in humans as well as in mice has been reported in the literature (Fig. 9) [21,22]. *In vivo* metabolism of [^{18}F]AV-45 in mice showed that, at 30 min after an intravenous injection, only 30% of the parent [^{18}F]AV-45 remained in the plasma. The biological half-life of [^{18}F]AV-45 in mouse plasma was estimated to be <30 min. Metabolite profiling and identification of the metabolites were done by HPLC with radioactive detection and liquid chromatography/mass spectroscopy analysis. Similar to that reported previously in mice and in humans several metabolites of [^{18}F]AV-45 were identified [21,22]. One of the major plasma metabolites was *N*-demethylated [^{18}F]AV-45 (designated as [^{18}F]AV-160), which constituted about 48% of the metabolites at 30 min after injection. The brain uptake of [^{18}F]AV-160 at 2 min after injection was 4.5%ID/g of tissue, and decreased to 1.8%ID/g at 60 min. The initial uptake of the parent [^{18}F]AV-45 was 1.5-fold higher than this metabolite. Also, a lipophilic metabolite, [^{18}F]AV-267, was identified. No significant binding to A β plaques was observed with either of the metabolites using AD brain-section autoradiography and the *in vitro* AD brain homogenate binding assay. The inhibition constants of AV-160 and AV-267 ($K_i = 54$ and 398 nM, respectively) indicate at least a 20–100 fold reduction of binding affinity to A β plaques in AD brain tissue homogenates, as compared with that of AV-45 ($K_i = 2.87$ nM). *N*-demethylation was also identified as main metabolic pathway in [^{18}F]AV-1 [42,43].

In vitro binding assay and *in vitro* autoradiography studies were used to measure [^{18}F]D3FSP affinity to β -amyloid plaques in the AD brain tissue homogenates. Because deuterium and hydrogen differ both in size

and hydrophobicity, it is possible that deuterated drugs bind more tightly to their biological targets. However, we found no change of binding affinity with deuterium substitution, and the effect, if any, was not measurable. Autoradiography of postmortem brain tissue sections with [^{18}F]D3FSP and [^{18}F]AV-45 was performed to support selective and specific binding of [^{18}F]D3FSP to A β plaques. [^{18}F]D3FSP showed high specificity in binding to β -amyloid plaques by *in vitro* homogenate binding assay and brain section autoradiography.

Generally, deuterated drugs retain their original biochemical potency and selectivity, but deuteration can produce substantial benefits to the overall pharmacological profile of the resulting compounds if corresponding C—H bonds are involved in critical steps in pharmacokinetics of drugs. Typically, cleavage of C—H bond is the starting point of *N*-demethylation and limiting *N*-demethylation might enhance the brain delivery. Biodistribution of [^{18}F]D3FSP in normal mice showed the ability of the tracer to rapidly cross BBB and rapid clearance from normal mice brain. Results of biodistribution of [^{18}F]D3FSP were comparable with those of [^{18}F]AV-45. Possible kinetic isotope effect in the metabolism of [^{18}F]D3FSP was limited to *N*-demethylation, which did not induce a pronounced overall deuterium kinetic isotope effect. Deuterium substitution of *N*-methyl group of AV-45 might not produce large enough effects in pharmacokinetics to modify the ultimate outcome in imaging β -amyloid plaques in the brain. Although [^{18}F]D3FSP did not yield a positive kinetic isotope effect, we have successfully created a new chemical entity which shows comparable preclinical properties to the FDA approved drug, [^{18}F]AV-45.

One other purpose of this research is to register a new β -amyloid plaque imaging agent for AD patients in China and other Asian countries

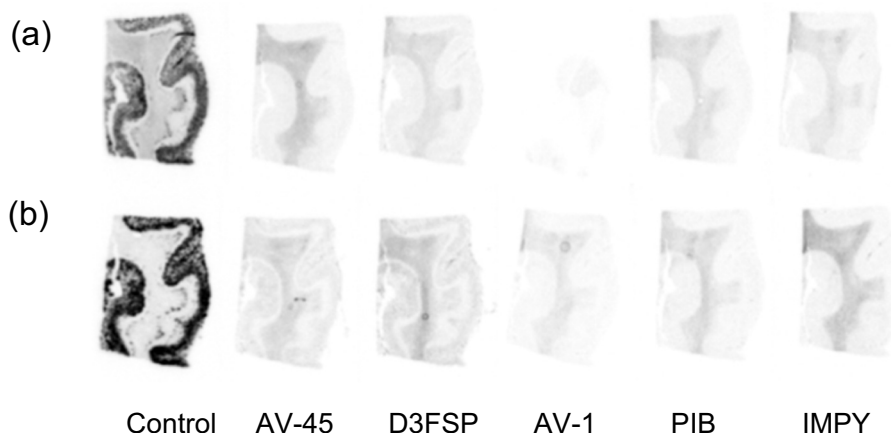


Fig. 5. Autoradiography images of postmortem AD brain slices by *in vitro* section labeling with (a) [^{18}F]AV-45 and (b) [^{18}F]D3FSP: control and blocking of β -amyloid plaque binding by various competing drugs. Concentrations of competing drugs were 1–5 μM .

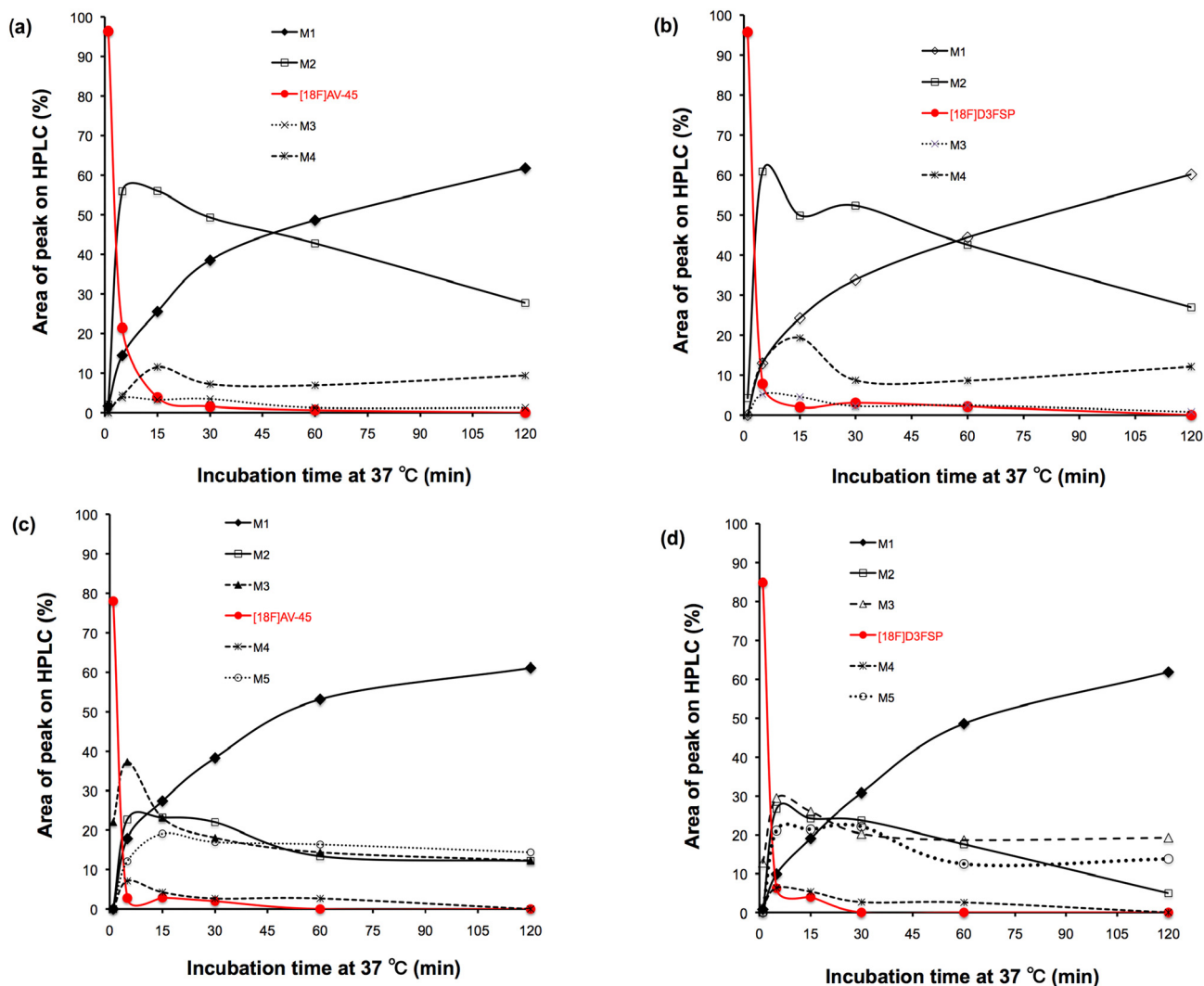


Fig. 6. Time-course of *in vitro* microsomal metabolism of (a) [^{18}F]AV-45 with mouse microsomes (b) [^{18}F]D3FSP with mouse microsomes (c) [^{18}F]AV-45 with human microsomes (d) [^{18}F]D3FSP with human microsomes. M1 is the corresponding *N*-demethylated [^{18}F]AV-45 or [^{18}F]D3FSP tracer. [^{18}F]AV-45 and [^{18}F]D3FSP displayed very similar *in vitro* metabolism profiles.

currently not served by the current FDA approved agents. Although, there are already three FDA approved β -amyloid plaque imaging agents available in the US, Japan and European countries, none of them has been successfully introduced in other markets. There is an enormous demand for β -amyloid plaque imaging in China and other Asian countries, because the current AD population is over ten million, which is likely more than the AD patients in the US and Europe combined. There is clearly an unmet clinical need in Asian countries and it would be entirely fair to develop one additional β -amyloid plaque imaging agent just for these countries. The new agent, [^{18}F]D3FSP, might serve as a clinical tool for assisting diagnosis and benefiting AD patients in

these countries currently not being served by the approved β -amyloid plaque imaging tracers.

[^{18}F]D3FSP displayed high specificity in binding to β -amyloid plaques similar to that observed for [^{18}F]AV-45 (Amyvid). *In vitro* and *in vivo* metabolism in mice suggested that both agents showed very similar pattern of metabolites, but deuterium substitution did not change *in vivo* metabolism. *In vivo* biodistribution in normal mice also exhibited very similar high brain penetration and rapid wash-out, a necessary property for effective brain imaging agents. It is reasonable to conclude that the hypothesis of improving the *in vivo* properties by using deuterated [^{18}F]D3FSP to reduce the *N*-demethylation did not

Table 2
Biodistribution of [^{18}F]D3FSP in wild type CD-1 mice (% dose/g, n = 3).

Organ	2 min	30 min	60 min	120 min
Blood	2.16 \pm 0.05	2.93 \pm 0.27	2.08 \pm 0.07	1.36 \pm 0.12
Heart	5.08 \pm 0.39	2.40 \pm 0.39	1.72 \pm 0.19	1.18 \pm 0.03
Muscle	3.21 \pm 0.14	1.79 \pm 0.06	1.20 \pm 0.04	0.75 \pm 0.07
Lung	4.88 \pm 0.16	2.90 \pm 0.47	1.97 \pm 0.25	1.31 \pm 0.03
Kidney	9.51 \pm 0.80	6.41 \pm 1.86	3.74 \pm 0.47	2.09 \pm 0.02
Spleen	2.50 \pm 0.12	1.52 \pm 0.21	1.22 \pm 0.12	0.83 \pm 0.07
Liver	12.00 \pm 0.70	11.99 \pm 0.71	8.15 \pm 0.75	5.47 \pm 0.29
Brain	6.26 \pm 0.23	1.71 \pm 0.37	1.53 \pm 0.20	1.26 \pm 0.04
Bone	1.74 \pm 0.18	2.24 \pm 0.44	2.76 \pm 0.37	4.41 \pm 0.77

Table 3
Biodistribution of [^{18}F]AV-45 in wild type CD-1 mice (% dose/g, n = 3).

Organ	2 min	30 min	60 min	120 min
Blood	2.28 \pm 0.15	3.27 \pm 0.27	2.39 \pm 0.46	1.66 \pm 0.24
Heart	4.22 \pm 0.58	2.54 \pm 0.31	2.03 \pm 0.13	1.51 \pm 0.24
Muscle	2.57 \pm 0.08	1.59 \pm 0.22	1.31 \pm 0.05	1.01 \pm 0.23
Lung	4.04 \pm 0.71	1.98 \pm 0.33	2.32 \pm 0.15	1.54 \pm 0.23
Kidney	9.60 \pm 0.96	8.52 \pm 1.17	5.79 \pm 1.53	2.67 \pm 0.49
Spleen	1.60 \pm 0.78	1.61 \pm 0.22	2.36 \pm 0.74	1.07 \pm 0.20
Liver	11.08 \pm 2.83	12.72 \pm 0.61	9.66 \pm 0.16	6.01 \pm 1.03
Brain	7.33 \pm 1.54	1.66 \pm 0.15	1.49 \pm 0.16	1.29 \pm 0.06
Bone	1.62 \pm 0.26	2.34 \pm 0.18	3.21 \pm 0.54	2.81 \pm 0.87

Table 4
Ratios of brain and blood uptake and clearance in normal mice.

	Brain 2 min/60 min	Blood 2 min/60 min	Brain/blood 2 min	Brain/blood 60 min
[¹⁸ F]D3FSP	4.1	1.0	2.9	0.7
[¹⁸ F]AV-45	4.9	1.0	3.2	0.6

work as originally envisioned. However, the new deuterium substituted agent, [¹⁸F]D3FSP, might be useful for imaging β -amyloid plaques in the brain. Recently, results of a phase I clinical study in humans (Dr. Dean Wong, Johns Hopkins University, un-published data, IND #137713, SNMMI abstract 2019) suggested that in the same AD patient [¹⁸F]D3FSP and [¹⁸F]AV-45 exhibited very similar patterns of brain distribution reflecting the β -amyloid plaque specific binding. However, there was no measurable delayed metabolic *N*-demethylation *in vivo* between [¹⁸F]D3FSP and [¹⁸F]AV-45 in AD patients suggesting that the original hypothesis could not be realized.

4. Conclusion

A new β -amyloid plaque targeting PET imaging agent, [¹⁸F]D3FSP - a *N*-trideuteromethyl (-NCD₃) analog of [¹⁸F]AV-45, was prepared and tested. *In vivo* and *in vitro* studies suggest that [¹⁸F]D3FSP binds to β -amyloid plaques with high affinity and displays a suitable pharmacokinetic characteristics comparable to [¹⁸F]AV-45. But the deuterium substitution did not lead to significant beneficial kinetic effects on slowing *in vivo* *N*-demethylation of [¹⁸F]D3FSP. However, results of preclinical studies suggest that [¹⁸F]D3FSP might be a suitable candidate as a new A β imaging agent to assist diagnosis of AD for a large patient population in countries currently not being served by FDA approved agents.

5. Materials and methods

Synthesis of D3FSP and related agents see Supplemental information.

5.1. Material

All reagents and solvents were purchased commercially (Aldrich, Acros, or Alfa Inc.) and were used without further purification, unless otherwise indicated. Solvents were dried through a molecular sieve system (Pure Solve Solvent Purification System; Innovative Technology, Inc.).

5.2. Radiosynthesis of [¹⁸F]D3FSP and [¹⁸F]AV-45

An activated Sep-Pak Light (Waters, Accell Plus QMA Carbonate) was loaded with [¹⁸F]fluoride (0.4–4.1 GBq) and eluted with

0.7 mL K₂₂₂/K₂CO₃ solution (40 mg K₂CO₃, 22 mg K₂₂₂, 18.4 mL ACN, 3.6 mL water) into a 1 mL conical vial. The solution was dried azeotropically twice with 1 mL acetonitrile at 80 °C. Ligand **4** (1.2 mg) was dissolved in 0.5 mL DMSO and added to the dried [¹⁸F]fluoride and vial was crimped. The mixture was heated for 15 min at 110 °C. The mixture was cooled at RT for 1 min; the vial was then opened and 250 μ L HCl (10%) was added and heated at 100 °C for 10 min. The reaction medium was added to 8 mL ice cold water, then 0.85 mL 1 N NaOH was added (final pH ~6). The mixture was loaded on an activated Oasis HLB 3 cc (60 mg) extraction cartridge. The cartridge was rinsed with 2 \times 3 mL water and the product was eluted with 1 mL ACN. The eluted acetonitrile solution was diluted with 1 mL water and injected into prep HPLC: Phenomenex Gemini C18, 250 \times 10 mm, ACN/water 60/40, 4 mL/min, 350 nm. The fraction at 11–12 min was collected. The fraction was diluted with 30 mL water and pushed through an activated Oasis HLB 3 cc (60 mg) extraction cartridge; the cartridge was washed with 3 mL water. The product was eluted with 1 mL EtOH (containing ascorbic acid). The ethanolic solution was concentrated under argon to about 100 μ L volume and diluted with 900 μ L saline. The ligand was evaluated by radio HPLC (Supelco Ascentis C18 150 \times 4.6, ACN/10 mM AFB (ammonium formate buffer) 50/50, 1 mL/min, 350 nm) ([¹⁸F]D3FSP: RCP: 98.5 \pm 1.3% (*n* = 8), RCY: 54 \pm 11% (decay corrected), molar activity (*A_m*): 22.8 \pm 12.4 GBq/ μ mol). Similarly, [¹⁸F]AV-45 and [¹⁸F]AV-1 were prepared with RCP: 98.4% (*n* = 6), RCY 46 \pm 8 (decay corrected), *A_m* = 22 \pm 14 GBq/ μ mol.

5.3. *In vitro* competitive binding assay

Competitive binding assays were performed in 12 \times 75 mm borosilicate glass tubes. The reaction mixture contained 100 μ L of AD brain homogenates (20–25 μ g), 100 μ L of [¹⁸F]AV-45 or [¹⁸F]D3FSP (~150,000 cpm), and 100 μ L of competing compounds (10⁻⁵ to 10⁻¹⁰ M diluted serially in PBS containing 0.1% bovine serum albumin) in a final volume of 250 μ L. Nonspecific binding was defined in the presence of 1 μ M of IMPY (6-iodo-2-(4'-dimethylamino-)phenyl-imidazo [1,2-*a*]pyridine) in the same assay tubes [41]. The mixture was incubated for 60 min at room temperature, and the bound and the free radioactivity were separated by vacuum filtration through Whatman GF/B filters using a Brandel M-24R cell harvester, followed by washing with PBS buffer three times. The radioactivity on the filters was counted with a gamma counter (Wizard², Perkin-Elmer). Data were analyzed using the nonlinear least-square curve fitting program LIGAND to determine IC₅₀. Ki was calculated by Cheng-Prusoff equation using 3.51 nM as Kd of AV-45 and D3FSP.

5.4. *In vitro* autoradiography AD brain section labeling of [¹⁸F]D3FSP

Frozen brains from AD and control subjects were cut into 20 μ m sections. The sections were incubated with [¹⁸F]D3FSP in 40% ethanol at a

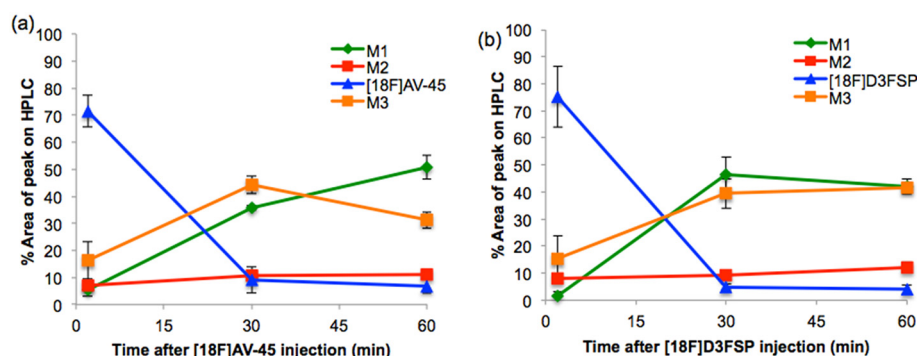


Fig. 7. Time-course of *in vivo* metabolism profiles of (a) [¹⁸F]AV-45 (b) [¹⁸F]D3FSP in the brain of normal mice: M1: Hydrophilic metabolite, M2: *N*-Demethylated AV-45 ([¹⁸F]AV-160), M3: Lipophilic metabolite ([¹⁸F]AV-267).

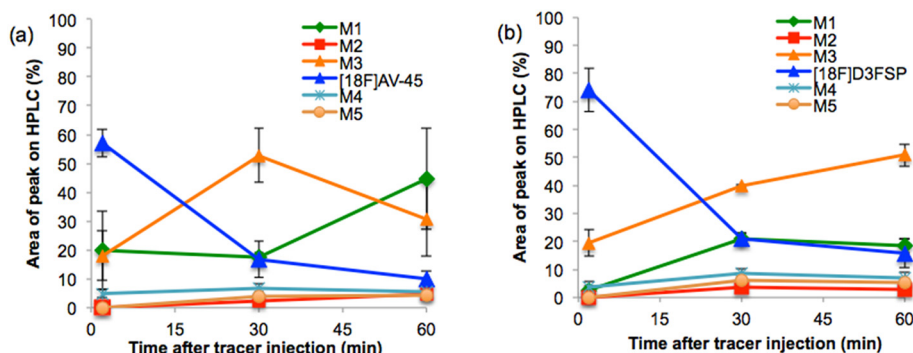


Fig. 8. Time-course of *in vivo* metabolism of (a) $[^{18}\text{F}]$ AV-45 (b) $[^{18}\text{F}]$ D3FSP in the plasma of normal mice: M1: Hydrophilic metabolite, M2: Hydrophilic metabolite, M3: *N*-Demethylated AV-45 ($[^{18}\text{F}]$ AV-160), M4: Lipophilic metabolite, ($[^{18}\text{F}]$ AV-267), M5: Lipophilic metabolite.

concentration of 0.3 nM for 1 h. The sections were then washed with 40% ethanol (2-min wash three times), followed by rinsing with water for 30 s. After drying, the sections were exposed to image plate for 30 min. Digitized images were acquired with Typhoon FLA 7000 (GE Healthcare).

5.5. *In vitro* liver microsomal metabolism

RapidStart™ NADPH regenerating system, human liver microsomes (Pool of 50, mixed gender, Lot No 1610016) and CD1 mouse liver microsomes (Pool of 1200, male, Lot No 1610148) were purchased from Sekisui XenoTech (Lenexa, KS). RapidStart™ NADPH regenerating system was reconstituted with 4 mL water. 25 μL of the NADPH-generating system, 2.22 MBq of $[^{18}\text{F}]$ D3FSP or $[^{18}\text{F}]$ AV-45 in 100 μL phosphate buffer solution, and 15 μL of human or mouse liver microsomes were employed in the study. The control vials were prepared by the same way without microsomes. The capped vials were gently shaken and placed in an incubator at 37 °C. At 1, 5, 15, 30, 60 and 120 min, 20 μL of the mixtures were quenched with 100 μL of acetonitrile, shaken vigorously for 10 s and centrifuged for 3 min at 5000 $\times g$. The acetonitrile layer was removed shortly before HPLC analysis. The RP-HPLC was performed using Agilent 1100 Series HPLC equipped with an Agilent XDB C18 column and the radiometric peaks were detected using a Bioscan flow detector.

5.6. Biodistribution in CD-1 mice

Animal studies were undertaken in compliance with University of Pennsylvania IACUC guidelines related to the conduct of animal experiments. CD-1 mice (20–26 g, male) were injected with $[^{18}\text{F}]$ D3FSP or $[^{18}\text{F}]$ AV-45 (720–925 kBq/mouse), 150 μL formulated in 10% ethanol and 90% saline directly into the tail vein. The mice were sacrificed by cardiac puncture under isoflurane anesthesia at various time points (2, 30, 60, and 120 min) after the injection. Organs of interest were removed and weighed, and the radioactivity was counted with a γ -counter. The injected percentage dose per organ was calculated by a comparison of the tissue counts to suitably diluted aliquots of the injected material. Each time point consisted of a group of 3 animals.

5.7. *In vivo* metabolites analysis by HPLC

Between 37 and 74 MBq of $[^{18}\text{F}]$ D3FSP or $[^{18}\text{F}]$ AV-45 was injected into the tail vein of CD-1 mice (three mice per each group). The mice were sacrificed at 2, 30 or 60 min after the injection. The blood samples were centrifuged at 2000 $\times g$ for 3 min to separate plasma. Plasma samples were mixed with equal volumes of acetonitrile followed by centrifugation at 5000 $\times g$ for 5 min to remove the denatured proteins. The supernatant was then analyzed directly by HPLC. The HPLC analysis was performed on an Agilent XDB-C18 column (150 \times 4.6 mm) with 0.1% trifluoroacetic acid in water and acetonitrile gradient at a flow

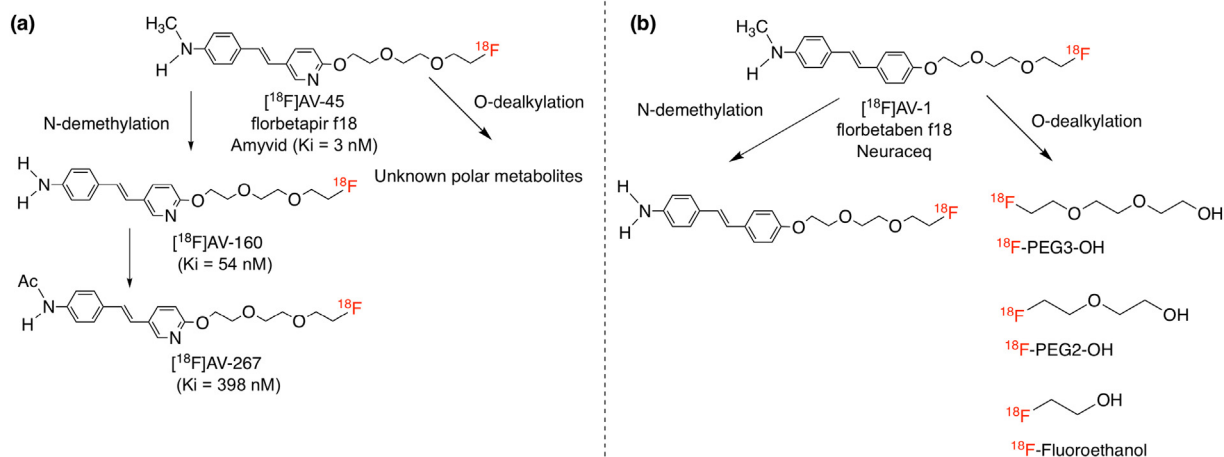


Fig. 9. Proposed metabolic pathways in humans of (a) $[^{18}\text{F}]$ AV-45 (florbetapir f18, Amyvid) by AVID Radiopharmaceuticals [44] and (b) $[^{18}\text{F}]$ AV-1 (florbetaben f18, Neuraceq) by Bayer Healthcare [45]. As indicated, one of the major metabolites were the *N*-demethylated derivatives for $[^{18}\text{F}]$ AV-45 and $[^{18}\text{F}]$ AV-1. The metabolites showed lower binding affinities to A β plaques in the brain.

rate of 1 mL/min. For the determination of metabolites in the brain, brain was homogenized in 1 mL of PBS and acetonitrile mixture. The homogenates were centrifuged at 5000 ×g for 5 min. The supernatant was separated from the tissue pellet, the supernatant was analyzed using HPLC. The retention times under these conditions were approximately 2.0 and 4.3 min for polar metabolites, 9.7 min for *N*-demethylated product, 10.9 min for parent ligand and 13.4 min and 16.6 min for lipophilic metabolites.

5.8. Pharmacological toxicity of D3FSP in normal rats

Studies were performed at Sai Life Sciences (Hinjawadi Phase II, Pune, Maharashtra 411057, India). Each treatment group was comprised of five each of male and female Sprague Dawley rats. Rats received either vehicle or 0.52 mg/kg D3FSP once on Day 1 *via* IV injection at a constant dosing volume of 4 mL/kg. This dose to rats represented 100× the maximum human dose that was assumed to be 50 µg, the same as AV-45. Clinical observations and body weight measurements were recorded daily. Blood samples for the evaluation of hematology, clinical chemistry, and coagulation endpoints were collected on Day 2 and Day 15. Following blood sample collections, necropsy was conducted. Protocol-specified tissues were collected from all animals and evaluated grossly, select organs were weighed, and tissues were fixed for microscopic evaluation. Tissues were subsequently processed and evaluated microscopically.

Abbreviations

AD	Alzheimer's disease
Aβ	β-amyloid, amyloid plaques
AV-1	Florbetapir f18
AV-45	Florbetapir f18
BBB	Blood-brain barrier
FDA	U.S. Food and Drug Administration
F-PIB	Flutemetamol f18
EMA	European medicines agency
KIE	Kinetic isotopic effect
IMPY	(2-(4'-dimethylaminophenyl)-6-iodo-imidazo[1,2- <i>a</i>]pyridine)
PET	Positron emission tomography
PIB	Pittsburgh compound B

Funding and disclosures

This research was supported by Five Eleven Pharma.

Compliance with ethical standards

Drs. Zha, Choi, Ploessl and Kung are inventors of a patent, in which [¹⁸F]D3FSP was part of the claims. Five Eleven Pharma holds the patent rights for D3FSP and related technology. The authors declare no other potential conflicts of interest.

Acknowledgments

Authors thank Dr. William Eckelman for insightful discussion and suggestions.

Appendix A. Supplementary data

Supplementary data to this article can be found online at <https://doi.org/10.1016/j.nucmedbio.2020.03.003>.

References

- Matthews KA, Xu W, Gaglioti AH, Holt JB, Croft JB, Mack D, et al. Racial and ethnic estimates of Alzheimer's disease and related dementias in the United States (2015–2060) in adults aged ≥/ =65 years. *Alzheimers Dement* 2019;15:17–24.
- Khachaturian AS, Hayden KM, Mielke MM, Tang Y, Lutz MW, Gustafson DR, et al. Future prospects and challenges for Alzheimer's disease drug development in the era of the NIA-AA research framework. *Alzheimers Dement* 2018;14:532–4.
- de Wilde A, van der Flier WM, Pelkmans W, Bouwman F, Verwer J, Groot C, et al. Association of amyloid positron emission tomography with changes in diagnosis and patient treatment in an unselected memory clinic cohort: the ABIDE project. *JAMA Neurol* 2018;75:1062–70.
- Veitch DP, Weiner MW, Aisen PS, Beckett LA, Cairns NJ, Green RC, et al. Understanding disease progression and improving Alzheimer's disease clinical trials: recent highlights from the Alzheimer's disease neuroimaging initiative. *Alzheimers Dement* 2019;15:106–52.
- van der Kant R, Goldstein LSB, Ossenkoppele R, Takeda S. Amyloid-beta-independent regulators of tau pathology in Alzheimer disease: progression of Alzheimer's disease, tau propagation, and its modifiable risk factors. *Nat Rev Neurosci* 2020; 21:21–35.
- Yang L, Rieves D, Ganley C. Brain amyloid imaging—FDA approval of florbetapir F18 injection. *N Engl J Med* 2012;367:885–7.
- Mallik A, Drzezza A, Minoshima S. Clinical amyloid imaging. *Semin Nucl Med* 2017; 47:31–43.
- Kung H, Choi S, Qu W, Zhang W, Skovronsky D. (18)F Stilbenes and styrylpyridines for PET imaging of abeta plaques in Alzheimer's disease: a minireview. *J Med Chem* 2009;53:933–41.
- Kung H. The β-amyloid hypothesis in Alzheimer's disease: seeing is believing. *ACS Med Chem Lett* 2012;3:265–7.
- Mathis CA, Mason NS, Lopresti BJ, Klunk WE. Development of positron emission tomography beta-amyloid plaque imaging agents. *Semin Nucl Med* 2012;42:423–32.
- Mathis CA, Lopresti BJ, Ikonovic MD, Klunk WE. Small-molecule PET tracers for imaging proteinopathies. *Semin Nucl Med* 2017;47:553–75.
- Lister-James J, Pontecorvo MJ, Clark C, Joshi AD, Mintun MA, Zhang W, et al. Florbetapir f-18: a histopathologically validated Beta-amyloid positron emission tomography imaging agent. *Semin Nucl Med* 2011;41:300–4.
- Yang L, Rieves D, Ganley C. Brain amyloid imaging—FDA approval of florbetapir F18 injection. *N Engl J Med* 2012;367:885–7.
- Golde TE, DeKosky ST, Galasko D. Alzheimer's disease: the right drug, the right time. *Science* 2018;362:1250–1.
- Johnson KA, Minoshima S, Bohnen NI, Donohoe KJ, Foster NL, Herscovitch P, et al. Update on appropriate use criteria for amyloid PET imaging: dementia experts, mild cognitive impairment, and education. *Amyloid Imaging Task Force of the Alzheimer's Association and Society for Nuclear Medicine and Molecular Imaging*. *Alzheimers Dement* 2013;9:e106–9.
- Jack Jr CR, Bennett DA, Blennow K, Carrillo MC, Dunn B, Haeblerlein SB, et al. NIA-AA research framework: toward a biological definition of Alzheimer's disease. *Alzheimers Dement* 2018;14:535–62.
- Rice L, Bisdas S. The diagnostic value of FDG and amyloid PET in Alzheimer's disease—a systematic review. *Eur J Radiol* 2017;94:16–24.
- Villemagne VL, Rowe CC. Long night's journey into the day: amyloid-beta imaging in Alzheimer's disease. *J Alzheimers Dis* 2013;33(Suppl. 1):S349–59.
- Selkoe DJ, Hardy J. The amyloid hypothesis of Alzheimer's disease at 25 years. *EMBO Mol Med* 2016;8:595–608.
- Chiao P, Bedell BJ, Avants B, Zijdenbos AP, Grand'Maison M, O'Neill P, et al. Impact of reference and target region selection on amyloid PET SUV ratios in the phase 1b PRIME study of aducanumab. *J Nucl Med* 2019;60:100–6.
- Wong D, Rosenberg P, Zhou Y, Kumar A, Raymond V, Ravert H, et al. In vivo imaging of amyloid deposition in Alzheimer disease using the Radioligand 18F-AV-45 (Flobetapir F 18). *J Nucl Med* 2010;51:913–20.
- Choi S, Golding G, Zhuang Z, Zhang W, Lim N, Hefti F, et al. Preclinical properties of 18F-AV-45: a PET agent for Aβ plaques in the brain. *J Nucl Med* 2009;50:1887–94.
- Senda M, Sasaki M, Yamane T, Shimizu K, Patt M, Barthel H, et al. Ethnic comparison of pharmacokinetics of (18)F-florbetaben, a PET tracer for beta-amyloid imaging, in healthy Caucasian and Japanese subjects. *Eur J Nucl Med Mol Imaging* 2015;42: 89–96.
- Choi SR, Schneider JA, Bennett DA, Beach TG, Bedell BJ, Zehntner SP, et al. Correlation of amyloid PET ligand florbetapir F 18 binding with abeta aggregation and neuritic plaque deposition in postmortem brain tissue. *Alzheimer Dis Assoc Disord* 2012; 26:8–16.
- Gant TG. Using deuterium in drug discovery: leaving the label in the drug. *J Med Chem* 2014;57:3595–611.
- Russak EM, Bednarczyk EM. Impact of deuterium substitution on the pharmacokinetics of pharmaceuticals. *Ann Pharmacother* 2019;53:211–6.
- Pirali T, Serafini M, Carginin S, Genazzani AA. Applications of deuterium in medicinal chemistry. *J Med Chem* 2019;62:5276–97.
- Timmins GS. Deuterated drugs: where are we now? *Expert Opin Ther Pat* 2014;24: 1067–75.
- Scheiner S. Calculation of isotope effects from first principles. *Biochim Biophys Acta* 2000;1458:28–42.
- Nag S, Fazio P, Lehmann L, Ketschau G, Heinrich T, Thiele A, et al. In vivo and in vitro characterization of a novel MAO-B inhibitor radioligand, 18F-labeled deuterated fluorodeprenyl. *J Nucl Med* 2016;57:315–20.
- Staley JK, Van Dyck CH, Tan PZ, Al Tikriti M, Ramsby Q, Klump H, et al. Comparison of [(18)F]altanserin and [(18)F]deuteroaltanserin for PET imaging of serotonin(2A) receptors in baboon brain: pharmacological studies. *Nucl Med Biol* 2001;28:271–9.

- [32] Nag S, Lehmann L, Ketschau G, Toth M, Heinrich T, Thiele A, et al. Development of a novel fluorine-18 labeled deuterated fluororasagiline ($[(18)\text{F}]\text{fluororasagiline-D2}$) radioligand for PET studies of monoamino oxidase B (MAO-B). *Bioorg Med Chem* 2013;21:6634–41.
- [33] Bonasera TA, Jonson SD, Pajeau TS, Katzenellenbogen JA, Welch MJ. Retardation of 17-oxidation of 16 alpha- $[(18)\text{F}]\text{fluoroestradiol-17 beta}$ by substitution of deuterium for hydrogen in the 17 alpha position(6). *Nucl Med Biol* 1997;24:239–49.
- [34] Schmidt C. First deuterated drug approved. *Nat Biotechnol* 2017;35:493–4.
- [35] Mullard A. Deuterated drugs draw heavier backing. *Nat Rev Drug Discov* 2016;15.
- [36] Guengerich FP. Kinetic deuterium isotope effects in cytochrome P450 reactions. *Methods Enzymol* 2017;596:217–38.
- [37] Kwicien RA, Molinie R, Paneth P, Silvestre V, Lebreton J, Robins RJ. Elucidation of the mechanism of N-demethylation catalyzed by cytochrome P450 monooxygenase is facilitated by exploiting nitrogen-15 heavy isotope effects. *Arch Biochem Biophys* 2011;510:35–41.
- [38] Sabri O, Seibyl J, Rowe C, Barthel H. Beta-amyloid imaging with florbetaben. *Clin Transl Imaging* 2015;3:13–26.
- [39] Kuchar M, Mamat C. Methods to increase the metabolic stability of $(18)\text{F}$ -radiotracers. *Molecules* 2015;20:16186–220.
- [40] Jahan M, Eriksson O, Johnstrom P, Korsgren O, Sundin A, Johansson L, et al. Decreased defluorination using the novel beta-cell imaging agent $[(18)\text{F}]\text{FE-DTBZ-d4}$ in pigs examined by PET. *EJNMMI Res* 2011;1:33.
- [41] Kung M, Hou C, Zhuang Z, Cross A, Maier D, Kung H. Characterization of IMPY as a potential imaging agent for b-amyloid plaques in double transgenic PSAPP mice. *Eur J Nucl Med Mol Imaging* 2004;31:1136–45.
- [42] Patt M, Schildan A, Barthel H, Becker G, Schultze-Mosgau MH, Rohde B, et al. Metabolite analysis of $[(18)\text{F}]\text{Florbetaben}$ (BAY 94-9172) in human subjects: a substudy within a proof of mechanism clinical trial. *J Radioanal Nucl Chem* 2010;284:557–62.
- [43] Fodero-Tavoletti MT, Brockschneider D, Villemagne VL, Martin L, Connor AR, Thiele A, et al. In vitro characterization of $[(18)\text{F}]\text{-florbetaben}$, an Abeta imaging radiotracer. *Nucl Med Biol* 2012;39:1042–8.
- [44] FDA. Amyvid (Florbetapir F18 injection). https://www.accessdata.fda.gov/drugsatfda_docs/nda/2012/202008_Florbetapir_Orig1s000TOC.cfm; 2012.
- [45] EMA. Neuraceq: florbetaben (18F). https://www.ema.europa.eu/documents/assessment-report/neuraceq-epar-public-assessment-report_en.pdf; 2014.